ORIGINAL PAPER

Oxidation of Stainless Steel Powder

Jinane Tarabay · Véronique Peres · Michèle Pijolat

Abstract To understand the corrosion behavior of a model 304L(p)–ZrO$_2$(s) composite, a 304L stainless steel powder was studied under oxygen at high temperature. Oxidation tests were performed with thermogravimetry. The so-called jumps method, which involves a sudden change of the temperature, was also applied to propose a kinetic model. Two periods with different rate-determining steps could be distinguished for short (<12 h) and long time experiments (12–20 h). SEM observations of oxidized particles revealed an oxide layer structure similar to that of alloy plates of same composition: during the first ten hours period, the external scale surrounding stainless steel particles was found to be chromium oxide; for the second oxidation period, the outer oxide layer was enriched in iron. Considering the relatively short-term oxidation period, a kinetic model based on an outward growth of chromia from oxidation of Cr in solution in the spherical alloy particles was successfully compared to the experimental mass gain curve. The k_p value deduced from this modeling was found to be in agreement with the literature data. The diffusion of interstitial chromium ions is the rate-determining step in agreement with the absence of influence of the oxygen partial pressure.

Keywords Powder · Stainless steel · Oxidation

J. Tarabay · V. Peres (✉) · M. Pijolat
Ecole Nationale Supérieure des Mines, SPIN-EMSE, CNRS:UMR 5307 LGF,
42023 Saint-Étienne, France
e-mail: peres@emse.fr

J. Tarabay
e-mail: tarabay@emse.fr

M. Pijolat
e-mail: mpijolat@emse.fr

Introduction

Ceramic matrix composites dispersed with metal particles, called M(p)–CMC(s) [1], are one of the promising materials for high performance applications under some severe environment such as high temperature. This new material design offers the possibility to combine heat resistance, corrosion resistance and wear resistance due to the ceramic phase, with mechanical strength and electric conductivity provided by the metal phase.

The oxidation at 800 °C of a model M(p)–CMC(s) composite based on zirconia and 304L stainless steel materials seem to be very complicated, a rapid mass gain occurs as soon as oxygen is introduced. After this short period the mass gain curves take a parabolic shape. To understand this unusual behavior, we decide to study the oxidation of the stainless steel powder alone.

This work based on thermogravimetry (TGA) experiments under 20 % O_2–80 % He at 1 atm presents the oxidation behavior at 800 °C of the stainless steel powder.

Experimental Procedures

The experiments were carried out on water-atomized 304L austenitic stainless steel powder provided by Hoganas Belgium. The chemical composition of the alloy established by the supplier is summarized in Table 1. Its specific surface area measured with the BET method is 0.06 m^2 g^{-1}. Various particle size classes, from 0 to 50 μm fraction up to a fraction >100 μm, have been obtained after sieving the steel powder.

The particle size distribution in volume, established by laser granulometry (Malvern instruments, Mastersizer 2000) reveals one main mode particle diameter at 80 μm (Fig. 1).

Test Facility and Conditions

Oxidation experiments were performed in a symmetric thermogravimetric analyzer (SETARAM TGA16 with a thermocouple PtRh 6 % /PtRh 30 %) at 800 °C for 6 h in a flowing mixture of helium and oxygen. The composition in oxygen was varied in the range 10–40 vol%. The tests were carried out at atmospheric pressure with a total gas flow rate of 2 L h^{-1} in each furnace. Samples consist of small beds (10 mg) of stainless steel powder placed in an alumina crucible.

The TGA experiments consisted of three main consecutive steps: heating to 800 °C with a rate of 30 °C min^{-1} under helium, isothermal exposure under oxygen helium mixture at 800 °C during various periods up to 20 h, cooling to room

Table 1 Chemical composition of 304L stainless steel

Weight (%)	Fe	Cr	Ni	Si
	Base	18.1	11.3	0.85

Fig. 1 Grain size distribution of 304L stainless steel powder
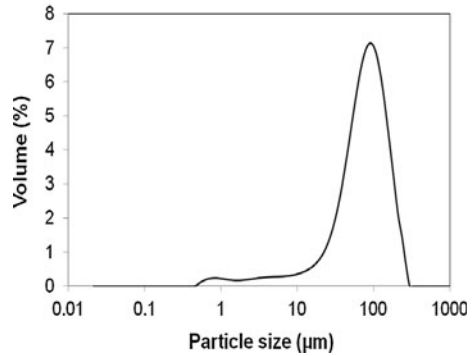
temperature with a rate of 30 °C min^{-1} under oxygen helium mixture. The oxygen is introduced after 7 min at 800 °C. The oxygen impurity in helium was analyzed at the outlet of the furnace by an oxygen probe (Systech Instruments Série 900) with an accuracy of about 1 ppm at 20 °C.

Results

TGA Results

A lack of reproducibility of the oxidation curves of 304L stainless steel powder is observed which is mainly due to a difference in particle size. The mass gain curves vs time for the as received 304L powder and for the various particles size classes are shown in Fig. 2. It can be seen that a good reproducibility was obtained with each
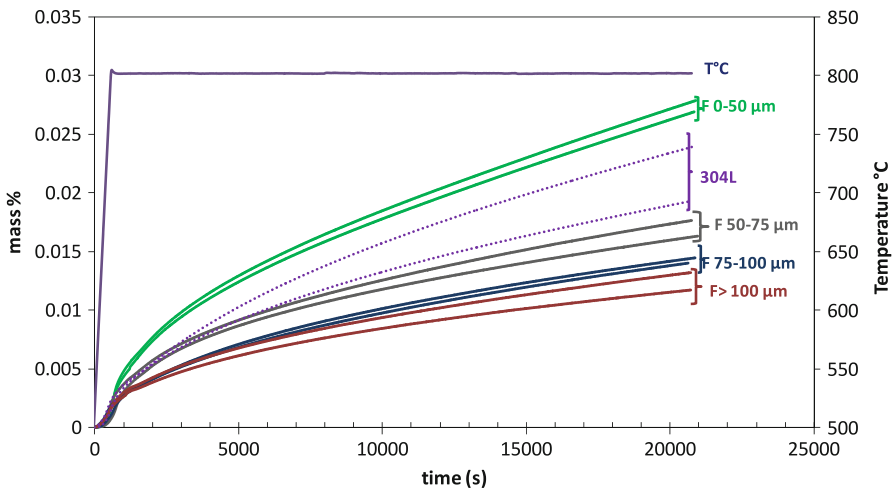

Fig. 2 Mass gain (%) versus time of as received and sieved 304L stainless steel powders oxidized at 800 °C (20% in volume of O_2 in helium)
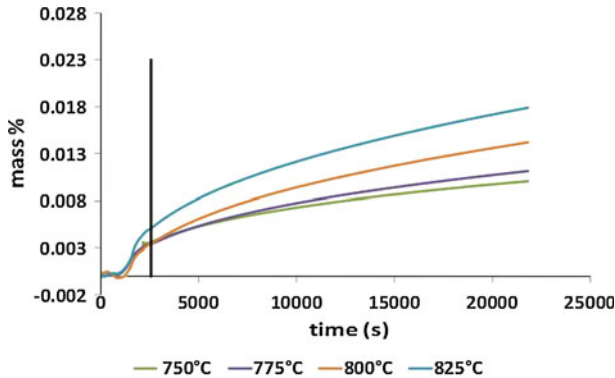
Fig. 3 Mass gain (%) versus time of 75–100 μm class of 304L stainless steel powder oxidized under 20 % in volume of O_2 at 750, 775, 800 and 825 °C

particle size class of sieved powders, whereas the curves obtained with the as received 304L powder were not so well reproducible.

The powder with the finest particles class (0–50 μm) shows greatest mass gain than the as received powder, while the largest one (>100 μm) shows least mass gain. The curves of the intermediate particle-size classes (50–75 μm and 75–100 μm) fall between those extreme curves. The reproducibility of the oxidation curves of the particle-size class (75–100 μm) is the best one, so this 304L stainless steel powder fraction has been used for the kinetic study.

The first part of the mass gain curves corresponds to the heating under helium up to the introduction of oxygen at the beginning of the plateau at 800 °C. The small mass change during the first period is due to oxygen traces in helium (50 ppm).

Figure 3 illustrates the mass gain curves versus time (under isobaric and isothermal conditions) for samples oxidized at different temperatures under 20 % in volume of O_2. As expected, the mass gain increases with the temperature increase.

Figure 4 illustrates the mass gain curves versus time (under isobaric and isothermal conditions) for samples oxidized at 800 °C under 10, 20 and 40 % in volume of O_2. The curves are superimposed; it means that there is no influence of oxygen partial pressure on the kinetic behavior of 304L stainless steel powder.

Characterization of 304L Stainless Steel Powder

Figure 5a and b show individual metal alloyed particles of stainless steel powder. A native Cr_2O_3 layer around the particles can be observed. During water-atomization the powder is oxidized [2, 3].

Figures 6a and b show SEM observations of the powder oxidized during respectively 6 and 20 h. The particles exhibit an external Cr_2O_3 layer growth surrounding the metallic particles. The scale begins to loose adherence after 20 h of oxidation. EDX analysis (Fig. 7) shows that the outermost layer is composed of an iron rich mixed oxide phase.
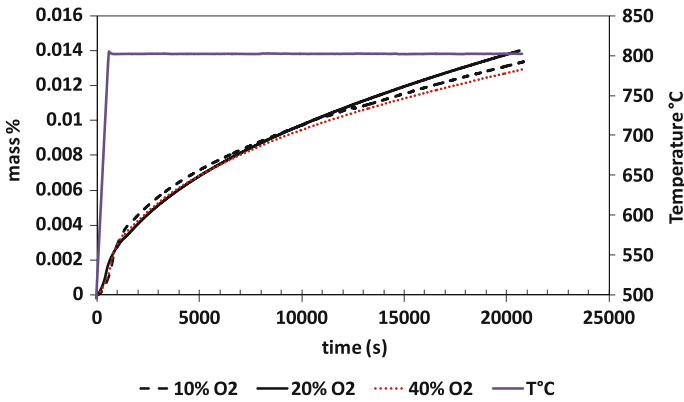
Fig. 4 Mass gain (%) versus time of 75–100 μm class of 304L stainless steel powder oxidized at 800 °C under 10 % (*black dotted line*), 20 % (*black continuous line*), 40 % (*red fine dotted line*) in volume of O_2 (Color figure online)
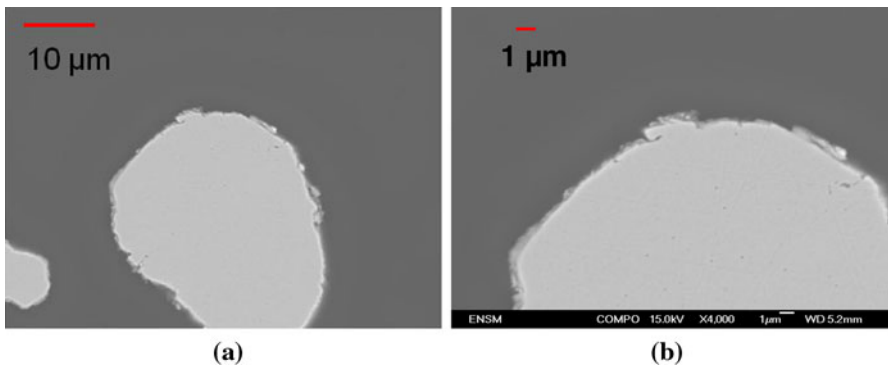

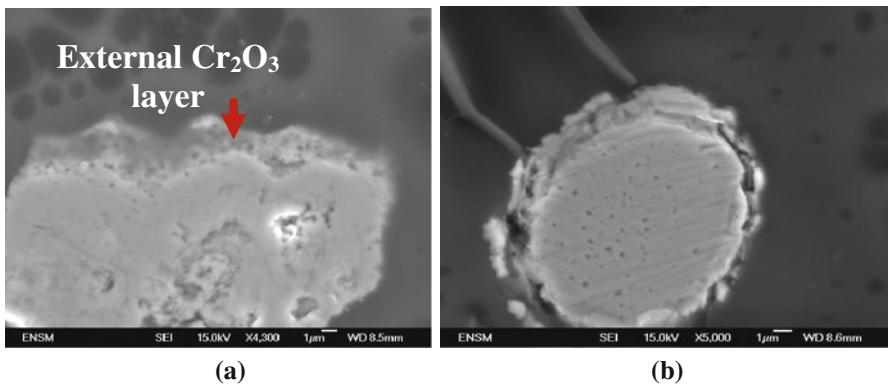**Fig. 5** SEM observations of starting 304L stainless steel powder

Fig. 6 SEM observations of 304L stainless steel powder oxidized at 800 °C after 6 h (**a**) and 20 h (**b**)
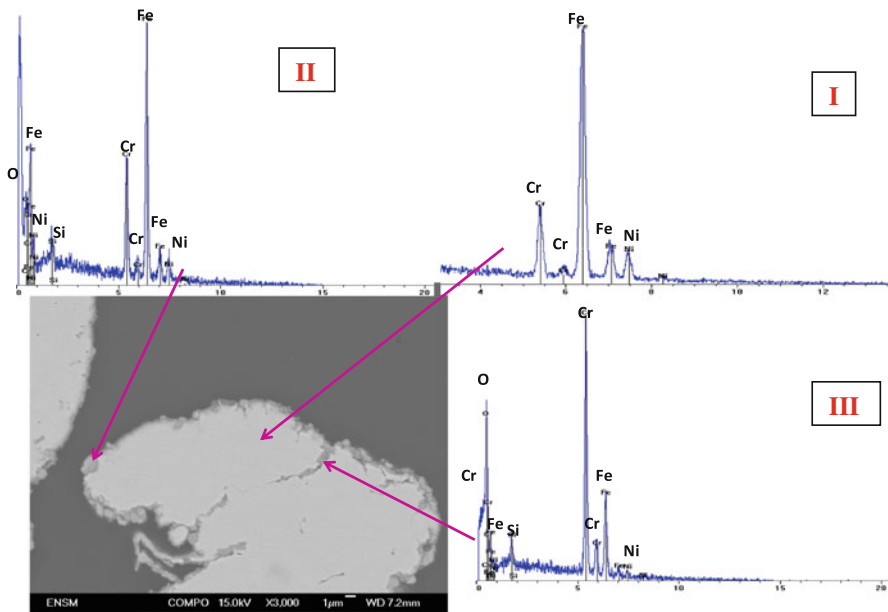
Fig. 7 EDX analysis of 304L stainless steel powder oxidized at 800 °C after 20 h

Discussion

The oxidation of 304L stainless steel powder shows a parabolic like behavior with an external Cr_2O_3 layer growth. According to literature data concerning the oxidation of 304L foils [4–6], the oxide growth should be controlled by the diffusion of cations. Assuming that the Cr_2O_3 layer remains very thin compared to the particle radii, a parabolic law could account for the experimental mass gain curves. Due to the existence of an initial native oxide layer, the complete parabolic law (Eq. 1) has been applied to the experimental data, the mass gain is normalized by the surface area of the powder (Fig. 8) [7]. The fitted value of k_p is equal to 2.5×10^{-12} g^2 cm^{-4} s^{-1} in agreement with the literature data for Cr_2O_3 growth (at 800 °C: $k_p = 8 \times 10^{-12}$ g^2 cm^{-4} s^{-1}) [8].

$$t = A + B\Delta m + \frac{1}{k_P}\Delta m^2 \tag{1}$$

However, a much more detailed kinetic analysis can be undertaken considering the kinetics of solid-gas reactions with powders. Solid gas reaction kinetic modeling is based on the assumption of the rate determining step which can be validated using the "ϕ S_m" test based on the jumps method [9, 10]. Such a method consists of a sudden jump in a thermodynamic variable (temperature or pressure) from an initial value to a final one and uses the ratios of the kinetic rates measured after/before this jump.

When the reaction is controlled by diffusion or by an interfacial step, the kinetic rate expressed as $d\alpha/dt$ (where α is the fractional conversion), is given by:
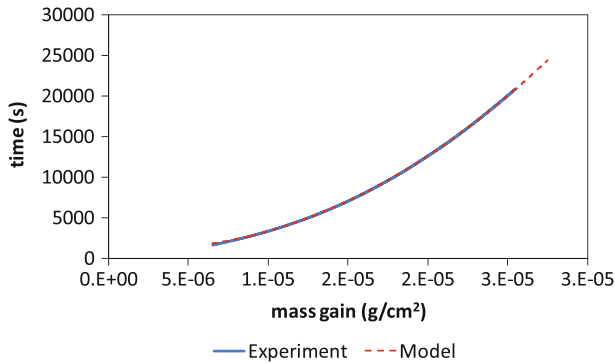
Fig. 8 Oxidation of 304L stainless steel powder at 800 °C: experimental curve and complete parabolic law

$$\frac{d\alpha}{dt} = \phi(T, Pi, \ldots) \cdot S_m(t) \qquad (2)$$

where ϕ (T, Pi,…) is the areic rate of growth (mol m^{-2} s^{-1}), and $S_m(t)$ is the space function (m^2 mol^{-1}) related to the extent of the reaction area where the rate-determining step takes place, which depends on the time and on the history of the solid. The jumps method was applied in our tests by a sudden change of the temperature from $T_0 = 780$ °C to $T_1 = 800$ °C at various mass gains. Figure 9 illustrates the ratio of the kinetic rates (R) after/before the jump versus mass gain. The "ϕ S_m" test is validated if the ratio of values does not depend of the mass gain at which the jumps are done. Figure 9 shows that we can consider two domains, in the first domain until 9 h the ratios take a constant value around 1.45 ± 0.05, in the second domain after 12 h of treatment the ratios are also constant, the value is higher around 2 ± 0.01. The "ϕ S_m" test is validated in both separate domains. In each of these areas the oxidation rate of 304L powder (75–100 μm) can be decomposed into a product functions according to Eq. (2). There is thus in both cases a step of the growth mechanism of the oxide which controls the speed of the reaction. However, after a certain oxidation time (from 12 h), a different rate-determining step and/or a different mechanism should be considered. Based on the literature and SEM/EDX observations of 304L powder oxidized after 6 and 20 h, we can assume that, at first, it is the diffusion of Cr^{3+} ions which determines the rate of reaction. Then from a certain thickness of chromium oxide, it is the diffusion of Fe^{3+} which limits the rate, the outer oxide layer becoming rich in iron.

Assuming an Arrhenius behavior for the dependence of ϕ with temperature, the activation energy calculated from the first domain ratio is about 177 kJ mol^{-1} which is rather similar to that of Cr/Cr_2O_3 reaction (158 kJ mol^{-1}) [11]. For the second domain, the apparent activation energy is about 322 kJ mol^{-1}. Consequently this higher apparent activation energy should correspond to the growth of the mixed oxide rich in iron.
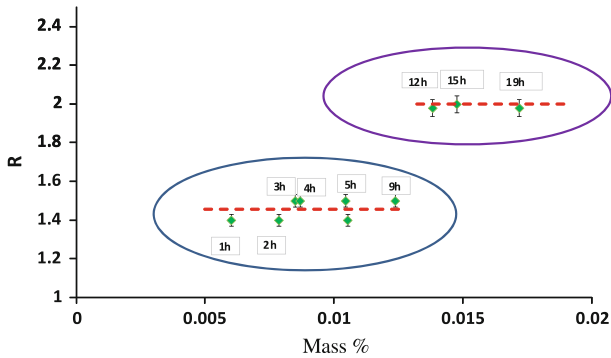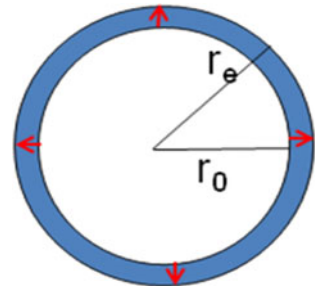
Fig. 9 Oxidation of 304L stainless steel powder: ratio R for jumps changes from 780 to 800 °C (20 % O$_2$)

Fig. 10 Scheme illustrating the oxide layer (thickness equal to $r_e - r_0$) around a spherical stainless steel powder particle with a r_0 initial radius

Kinetic Model

In the first domain (short oxidation time), the rate law can be obtained using the assumption that the rate-determining step corresponds to the external Cr$_2$O$_3$ oxide layer growth around the stainless steel powder particles, considered as spherical (Fig. 10). The oxidation is controlled by the diffusion of Cr cations through the oxide layer.

The rate law is given by:

$$\frac{d\alpha}{dt} = J_{Cr} \cdot \frac{s}{n_0} \tag{3}$$

where s is the initial surface of a stainless steel particle, n_0 is the initial mole number of Cr in the 304L stainless steel and J_{Cr}, the diffusion flow in mol m^{-2} s^{-1}, is given by:

$$J_{Cr} = D_{Cr}|\Delta C| \frac{r_e}{r_0(r_e - r_0)} \tag{4}$$

where D_{Cr} is the diffusion coefficient of Cr in m^2 s^{-1}, ΔC is the difference in the Cr concentration at both sides of the diffusion layer.

Knowing that the fractional conversion α represents the ratio between the experimental mass obtained from TGA and the theoretic mass necessary for total oxidation of chromium in the stainless steel (18 wt%), α the fractional conversion can be written by:

$$\alpha = \frac{n_{Cr_2O_3}}{\frac{1}{2}n_0} = \frac{2}{n_0 \cdot V_{m_{ox}}} \cdot \left(\frac{4}{3} \cdot \pi \cdot r_e^3 - \frac{4}{3} \cdot \pi \cdot r_0^3\right) \tag{5}$$

where n_0 is the mole number of Cr in the sample of powder of mass m_0

$$n_0 = \frac{m_0 \cdot 0.18}{M_{Cr}} \tag{6}$$

and $n_{Cr_2O_3}$ is the mole number of Cr_2O_3 formed, V_{mox} is the molar volume of Cr_2O_3. From Eq. (5), r_e can be expressed by:

$$r_e = r_0 \left(1 + \frac{3 \cdot n_0 \cdot V_{m_{ox}} \cdot \alpha}{8 \cdot \pi \cdot r_0^3}\right)^{1/3} \tag{7}$$

with r_0 the mean radius equal to 43 microns considering the T-304L stainless steel powder (75–100 μm) particles as spherical. Thus the rate law can be written as:

$$\frac{d\alpha}{dt} = \phi \cdot \frac{4 \cdot \pi \cdot r_0}{n_0} \frac{\left(1 + \frac{3 \cdot n_0 \cdot V_{m_{ox}} \cdot \alpha}{8 \cdot \pi \cdot r_0^3}\right)^{1/3}}{\left[\left(1 + \frac{3 \cdot n_0 \cdot V_{m_{ox}} \cdot \alpha}{8 \cdot \pi \cdot r_0^3}\right)^{1/3} - 1\right]} \tag{8}$$

In this expression, α the fractional conversion is the ratio of the experimental mass change Δm relative to the mass variation theoretically needed to oxidize the chromium in the alloy. The value of α can be calculated from the experimental mass change Δm versus time according to Eq. (9):
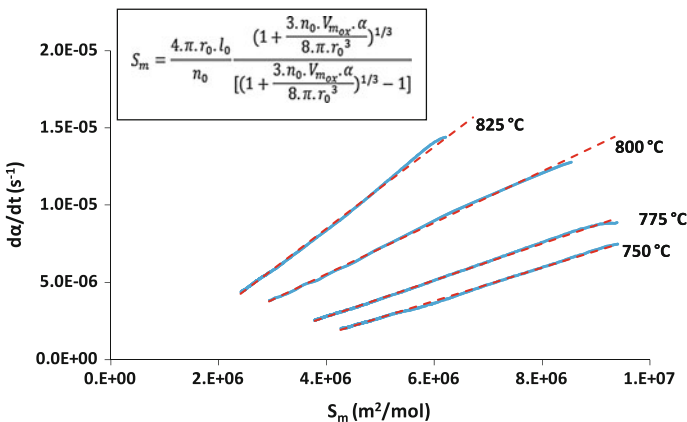

Fig. 11 Oxidation of 304L stainless steel powder : experimental data (*blue continuous lines*) and theoretical rate laws (*red dotted lines*) (Color figure online)

$$\alpha = \frac{\Delta m}{\Delta m_{th}} = \frac{\Delta m}{\frac{3}{4} \cdot M_{O_2} \cdot n_0} \tag{9}$$

with M_{O_2} the oxygen molecular weight.

Figure 11 represents the fits between the kinetic data ($d\alpha/dt$) and the theoretical rate law considering S_m function [cf. Eqs. (2) and (8)].

Only the kinetic data corresponding to the first oxidation domain between 0 and 9 h give a straight line whose the slope of $d\alpha/dt = \phi S_m$ give the value of ϕ at each temperature. The model is thus found in good agreement with experimental data.

Table 2 shows the values of ϕ for temperatures between 750 and 825 °C.

Based on these data, and plotting $\ln \phi$ as a function of $1/T$ (Fig. 12), a straight line is obtained with an acceptable coefficient of correlation showing that ϕ depends on the temperature according to the Arrhenius law. The apparent activation energy obtained is equal to 139 kJ / mol. This value is significantly lower than that of the value previously calculated from the ratio of the kinetic rates in the short time period (cf. Figure 9), but nevertheless, the two methods of calculation give values of apparent activation energy close to 158 kJ / mol, which correspond to the system Cr/Cr_2O_3.

Relation Between ϕ and k_p

ϕ and k_p are temperature dependent and they represent quantities obtained for the same diffusion controlling step but in different geometries (spheres and plates respectively). In a planar geometry, the fractional conversion α is given by:

Table 2 ϕ values at different temperatures

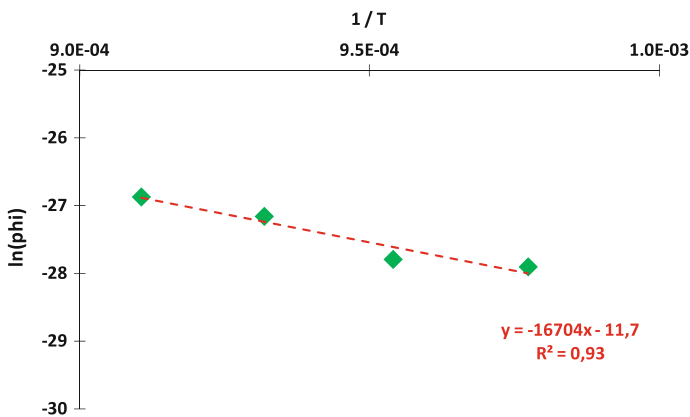| Temperature (°C)	ϕ (mol m^2 s^{-1}) $\times 10^{-12}$
750	0.76
775	0.85
800	1.59
825	2.13

Fig. 12 Variation of $\ln \phi$ versus $1/T$ (K^{-1})

$$\alpha = \frac{4}{3} \cdot \frac{1}{n_0 M_{O_2}} \cdot \Delta m \tag{10}$$

The kinetic rate is given by:

$$\frac{d\alpha}{dt} = \phi \cdot S_m = \phi \cdot \frac{l_0}{x} \cdot \frac{\varepsilon}{n_0} \tag{11}$$

where l_0 is a length equal to unity (1 m), X is the thickness of the oxide layer expressed by Eq. (12):

$$X = \frac{2 V m_{ox}}{3 M_{O_2}} \cdot \frac{\Delta m}{s} \tag{12}$$

The relationship between k_p and ϕ is established from the combination of Eq. (11) and of the derivative of Eq. (1),

$$k_p = \frac{l_o 3^2 M_{O_2}^2}{4 V m_{ox}} \phi \tag{13}$$

At 800 °C, based on the value of ϕ, k_p is equal to 2×10^{-12} g^2 cm^{-4} s^{-1}. This value is in good agreement with the value found using the complete parabolic law: $k_p = 2.5 \times 10^{-12}$ g^2 cm^{-4} s^{-1} and with literature data confirming the similar behavior between 304L plates and powder.

Conclusions

This study has put in evidence a conventional oxidation of the 304L stainless steel powder with a parabolic like behavior. The fitted k_p value calculated with a complete parabolic law is similar to literature data. From the jumps method, two distinct rate-determining steps were observed for short (<12 h) and long (>12 h) oxidation times at 780–800 °C. Based on bibliographic data and SEM analysis, the first period was attributed to the outward oxidation of Cr forming an external Cr_2O_3 layer, while the second period was attributed to the growth of an iron-rich mixed oxide at the outermost oxide scale. A kinetic model devoted to the oxidation in Cr in solution in spherical particles of 304L was established and allowed to fit the short oxidation kinetic data. The k_p value deduced from this model was in agreement with the literature data obtained for plates, indicating a similar behavior of the 304L stainless steel powder.

This study will help us to understand the unusual oxidation behavior of a model composite elaborated with 304L stainless steel particles inserted in an yttrium stabilized zirconia matrix which seems to play a basic role in the early stage of the composite oxidation process.

References

1. M. Nanko, *Science and Technology of Advanced Materials* **6**, 129 (2005).
2. A. Nylund, T. Tunberg, H. Bertilsson, E. Carlstrom, and I. Olefjord, *The International Journal of Powder Metallurgy* **31**, 365 (1995).
3. M. Norell, A. Nyborg, T. Tunberg, and I. Olefjord, *Surface and Interface Analysis* **19**, 71 (1992).
4. V. Alenka, M. Mozetic, and A. Zalar, *Applied Surface Science* **200**, 94 (2002).
5. H. Asteman, J. E. Svensson, and L. G. Johansson, *Oxidation of Metals* **57**, 193 (2002).
6. F. Riffard, H. Buscail, E. Caudron, R. Cueff, C. Issartel, S. ElMesski, and S. Perrier Materials, *Science Forum* **461–464**, 175 (2004).
7. D. Monceau and B. Pieraggi, *Oxidation of Metals* **50**, 477 (1998).
8. P. Kofstad, *High-Temperature Corrosion* (Elsevier, London, 1988).
9. M. Pijolat and M. Soustelle, *Thermochimica Acta* **478**, 34 (2008).
10. K. Surla, F. Valdivieso, M. Pijolat, M. Soustelle, and M. Prin, *Solid State Ionics* **143**, 355 (2001).
11. D. Young, *High Temperature Oxidation and Corrosion of Metals* (Elsevier, Amsterdam, 2008).